Characterization of Martensite-Austenite Constituents and Micro-hardness in Intercritical Reheated and Coarse-grained Heat Affected Zone of API X70 HSLA Steel

M. Mohammadijoo[a,b], Jonas Valloton[a], L. Collins[b], H. Henein[a], D.G. Ivey[a*]

[a]Department of Chemical and Materials Engineering, University of Alberta, Edmonton, AB, Canada T6G 1H9

[b]R&D Division, Evraz Inc. NA, P.O. Box 1670, Regina, SK, Canada S4P 3C7

*Corresponding author: Prof. Ph.D.; Tel.: +1 780 4922957; Fax: +1 780 4922881

E-mail address: divey@ualberta.ca (D.G. Ivey)

Abstract

The thermal cycles that high strength low alloy (HSLA) low carbon steels experience during welding inevitably affect the microstructure and mechanical properties of the weld joints. It is generally agreed that the coarse-grained heat affected zone (CGHAZ) and the intercritical reheated coarse-grained heat affected zone (ICRCGHAZ) in one-pass and multi-pass welding, respectively, have the poorest microstructure and mechanical properties relative to the rest of the steel joint. The martensite-austenite (M-A) constituents formed in the HAZ regions predominantly govern property deterioration in the CGHAZ and the ICRCGHAZ by promoting the initiation and propagation of micro-cracks. However, the characteristics of the M-A constituents, i.e., fraction, size, shape and aspect ratio, are strongly affected by the welding heat input. Accordingly, in this study, the aim was to evaluate the influence of a cold wire addition in conventional tandem submerged arc welding (TSAW+cold-wire) on the microstructure and micro-hardness in the CGHAZ and ICRCGHAZ. Microstructural characterization showed that a lower fraction of finely distributed fine M-A constituents associated with smaller prior austenite grains (PAGs) formed in the CGHAZ of the steel welded by the TSAW+cold-wire process (CW-OD weld) relative to that welded by the conventional TSAW process (TW-OD weld). Furthermore, the fraction of M-A constituents in the ICRCGHAZ of the CW-OD weld was decreased. A higher fraction of slender shape M-A constituents in the ICRCGHAZ of the TW-OD weld resulted in an increase in the micro-hardness. The microstructure and micro-hardness changes associated with cold wire addition were attributed to the lower welding heat input and, consequently, the faster cooling rate with a corresponding reduction in the retention time in the austenitic region and ferrite/austenite region in the CGHAZ and ICRCGHAZ regions, respectively.

Keywords: Micro-hardness; Martensite-austenite; Intercritical reheated HAZ; HSLA steel

1. Introduction

Microalloyed steels are a class of high strength low alloy (HSLA) steels with low carbon content as well as low amounts of alloying elements, such as niobium, titanium and vanadium. These steels are extensively used for manufacturing pipelines, pressure vessels and automobiles due to their exceptional combination of strength and toughness. Welding of these steels is essential for manufacturing, which inevitably affects the structural performance of the final product as a result of the thermal cycles that the steel experiences during welding. In fact, there is general agreement that the probability of failure within the heat-affected zone (HAZ) is much higher than for the rest of the steel joint. This is mainly due to the microstructural alterations in the HAZ taking place during welding. However, along the HAZ there are two regions with the poorest mechanical properties, particularly fracture toughness. The coarse-grained heat affected zone (CGHAZ) and the intercritical reheated coarse-grained heat-affected zone (ICRCGHAZ) in one-pass and multi-pass welding, respectively, have the poorest fracture toughness relative to the rest of the steel. The property deterioration is essentially dependent on microstructural constituents formed in the CGHAZ and the ICRCGHAZ [1–6]. The formation of large prior austenite grains (PAGs) along with martensite-austenite (M-A) constituents in the CGHAZ and the formation of a "necklace" structure of M-A constituents along the prior austenite grain (PAG) boundaries in the ICRCGHAZ, which are highly dependent on welding heat input, are believed to promote the initiation and propagation of micro-cracks.

Haugen et al. [1] reported that the formation of M-A phases along the PAG boundaries and a mixture of bainite/tempered martensite within the PAGs caused reduction in ICRCGHAZ fracture toughness. Di et al. [3] reported that the volume fraction and size of M-A constituents were the key factors for toughness deterioration in the ICRCGHAZ. The work done by Hu et al. [7] showed that the carbon content of the M-A constituents plays a significant role in the deterioration of mechanical properties in the ICRCGHAZ. They found that the addition of vanadium and nitrogen in the steel leads to the formation of VN precipitates during the first welding pass which provides potential nucleation sites for ferrite, leading to refinement of M-A constituents. In addition, the formation of a high density of V(C,N) precipitates consumes the carbon content in the austenite, leading to an decrease in the carbon content of M-A constituents. These effects result in a reduction in the hardness and an improvement in the toughness of the ICRCGHAZ.

Han et al. [8] reported that the strength in the ICRCGHAZ increases with an increase in the fraction of M-A islands. However, the M-A islands act as crack initiation sites in the HAZ of HSLA steels, which result in toughness deterioration [9]. Kweon et al. [10] have reported that fracture toughness decreased in the ICRCGHAZ with increasing intercritical peak temperature of the second welding pass. This was due to the formation of a higher fraction of larger M-A constituents. It was suggested by Moeinifar et al. [11] that a reduced fraction of M-A constituents in the ICRCGHAZ is beneficial to the impact toughness. With reference to the CGHAZ, Davis et al. [12] found that the formation of enlarged M-A constituents along the

PAG boundaries resulted in cleavage crack initiation in the HAZ. It was proposed that the formation of a continuous network of elongated M-A constituent results in an "overlap of transformation-induced residual tensile stresses" and, thus, an enhancement of the stress concentration due to the strength mismatch between the M-A and the matrix. As such, a network of inter-connected slender shaped M-A is detrimental to toughness. Xu et al. [13] reported that the ratio of martensite to austenite in M-A constituents increased with increasing welding heat input. Yu et al. [14] showed that the fraction of M-A constituents increased by coarsening the PAG size in the CGHAZ. They found that a coarse PAG size, associated with coarse M-A constituents, is the dominant factor in promoting brittle behavior of the CGHAZ. This finding was in accordance with the results reported by Gharibshahiyan et al. [15]. In fact, a large PAG size results in an increase in the martensite start temperature (Ms), which subsequently results in a higher volume fraction of martensite in the CGHAZ [16,17].

Accordingly, it is generally accepted that the characteristics of the M-A constituents, i.e., fraction, size, shape (blocky or slender) and aspect ratio (length/width), in both the ICRCGHAZ and CGHAZ regions, which are significantly impacted by the welding heat input, play a significant role on the HAZ mechanical properties. As such, in this paper the characteristics of the M-A constituents and micro-hardness of the ICRCGHAZ and CGHAZ of a typical HSLA steel welded by a recently developed welding process, i.e., tandem submerged arc welding (TSAW) with an additional cold wire (TSAW+cold-wire process), is evaluated and compared with those of a steel welded by the conventional TSAW process. The developed process essentially reduces the welding heat input by consumption of the heat of the trail electrode through addition of an electrically cold wire. The details of the welding process can be found in [18]. The consequent reduction in the heat input and increase in the cooling rate by the additional cold wire results in the changes in the microstructure and properties of the HAZ. Microstructure in both the ICRCGHAZ and CGHAZ is characterized using transmission electron microscopy (TEM), scanning electron microscopy (SEM), electron backscattered diffraction (EBSD) and tint etching optical microscopy (TEOM). To evaluate the influence of the M-A constituent on the properties, micro-hardness mapping is performed along the HAZ of welded specimens.

2. Experimental Procedure

2.1. Weld Sample Preparation

Two inner-diameter (ID) and outer-diameter (OD) welding runs (Fig. 1a) were conducted on V-shape beveled X70 (yield strength of 70 ksi or 482 MPa) HSLA microalloyed steel plates with a thickness of 13.4±0.3 mm, manufactured through thermo-mechanical controlled processing (TMCP) [19]. The bevel geometry machined in the steel plates is shown in Fig. 1b. Two 4 mm diameter EA2 electrodes and one electrically cold wire with the same diameter and composition were chosen according to ASME-SFA5.23

for arc generation and filling of the bevel. Direct current electrode positive and square wave alternating current polarity were employed, using constant current type power sources to operate the lead and trail electrodes in the OD weld run, respectively. Both the lead and trail electrodes in the ID weld run were operated in square wave alternating current polarity. A granular flux was chosen according to EN 760 (BF6.5, Bavaria, Germany) to shield the arc from the atmosphere. Table 1 shows the chemistry of the microalloyed steel and consumable electrodes. The Pcm value in Table 1 indicates the welding crack susceptibility index for low carbon microalloyed steels and was calculated according to the Ito-Bessyo equation [20]. Accordingly, the steel with Pcm value less than 0.35 wt.% has an excellent weldability with a relatively low susceptibility to cracking.

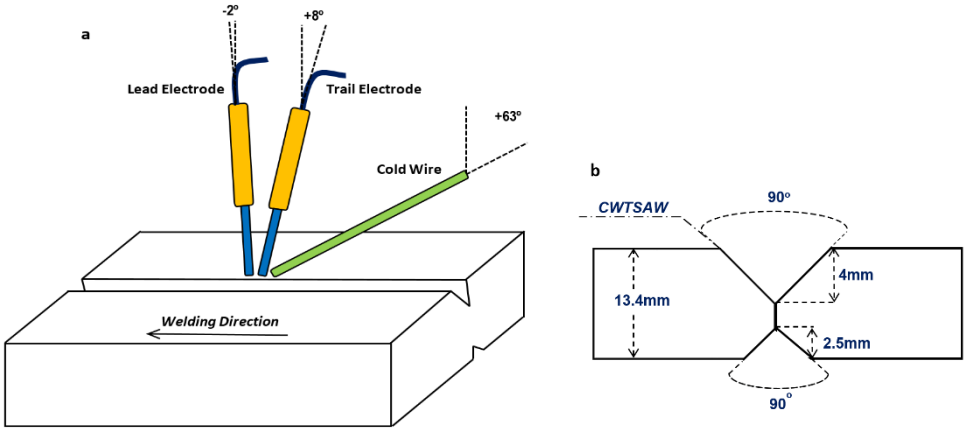

Figure 1. (a) Schematic of the TSAW+cold-wire process with positioning of the electrodes and cold wire and (b) X70 steel joint geometry indicating both ID and OD bevels.

Table 1. Composition of X70 microalloyed steel and electrode (wt%)

X70 Steel	**C**	**N**	**V+Mo+Nb+Ti**	**P**	**S**	**Mn**	**Si**	**Cu+Ni+Cr**	**Pcm***
	0.047	0.0096	0.22	0.01	0.001	1.74	0.24	0.53	0.175
Electrode Cold Wire (BA-S2Mo)	**C**	**P**	**S**	**Mn**	**Si**	**Mo**	**Ni**	**Cr**	**Cu**
	0.10	0.007	0.01	1.04	0.1	0.56	0.02	0.03	0.03

The goal was to specifically evaluate the influence of cold wire addition on the OD welding pass (intercritically reheating temperature) on the microstructural characteristics and the micro-hardness of the ICRCGHAZ. Accordingly, as shown in Table 2, the welding parameters for the ID weld run (performed via TSAW) were similar for both weld samples; only the OD welding parameters varied. The nominal heat input of the ID and OD welds for both welding processes was constant and set at 17.9 kJ/cm and 22.2 kJ/cm, respectively; however, as stated earlier, cold wire addition results in a reduction in the actual welding heat input of the OD weld. All welding parameters were the same for both processes other than the additional cold wire.

Table 2. ID and OD welding process parameters

Process Parameter	Units	ID-TSAW (**TW-ID weld**)	OD-TSAW+cold-wire (**CW-OD weld**)	OD-TSAW (**TW-OD weld**)
Current- Lead Electrode	amp	880	1040	1040
Current- Trail Electrode	amp	770	830	830
Voltage- Lead Electrode	volt	28	30	30
Voltage- Trail Electrode	volt	30	34	34
Welding Travel Speed	cm/min	160	160	160
Cold Wire Position	--	NA	Lagging	NA
Cold Wire Angle	°	NA	63	NA
Cold Wire Feed Speed	cm/min	NA	25.4	NA

2.2. Microstructure and Micro-hardness

Three weld coupons were cut along each weld in the transverse direction relative to the weld direction to examine the micro-hardness and characterize the microstructure in the CGHAZ and ICRCGHAZ of the OD and ID welds, respectively. Prior to micro-hardness mapping, the weld specimens were polished and etched according to ASTM E3-11 [21]. Vickers micro-hardness testing was conducted according to ASTM E384-11 [22]. SEM (Tescan-Vega-3) and TEOM (Olympus-BX61) were used to characterize overall microstructural alterations taking place in both the HAZ regions of the two welds. For this purpose, the freshly polished specimens were tint etched using modified LePera's etchant [23] for 30-50 s to reveal microstructural features in different colors. TEM and EBSD analyses were conducted to characterize particularly the M-A constituents, using a JEOL 2010 TEM (200 kV) equipped with an energy dispersive X-ray (EDX) spectrometer and a Zeiss Sigma field emission gun SEM (20 kV) equipped with an HKL EBSD system, respectively. TEM specimens were extracted from the ICRCGHAZ region using focused ion beam (FIB) methods. Quantitative analysis of the M-A constituent was done using ImageJ commercial image analysis software.

3. Results and Discussion

3.1. Micro-hardness Mapping

Micro-hardness mapping within the HAZ and ICRCGHAZ of both the TW-OD and CW-OD weld specimens is indicated in Fig. 2a and b, respectively. The micro-hardness value of the as-received X70 base steel was measured as 226±2 HV. As shown in Fig. 3, for a given welding process, the average micro-hardness of the ICRCGHAZ and CGHAZ was higher than that for the base steel; however, the micro-hardness of the ICRCGHAZ was higher than that of the CGHAZ for the same type of the weld sample. With reference to the weld specimen fabricated with the TSAW process and additional cold wire (CW-OD

weld), the micro-hardness mapping indicated a reduction in the micro-hardness value in both the ICRCGHAZ and CGHAZ.

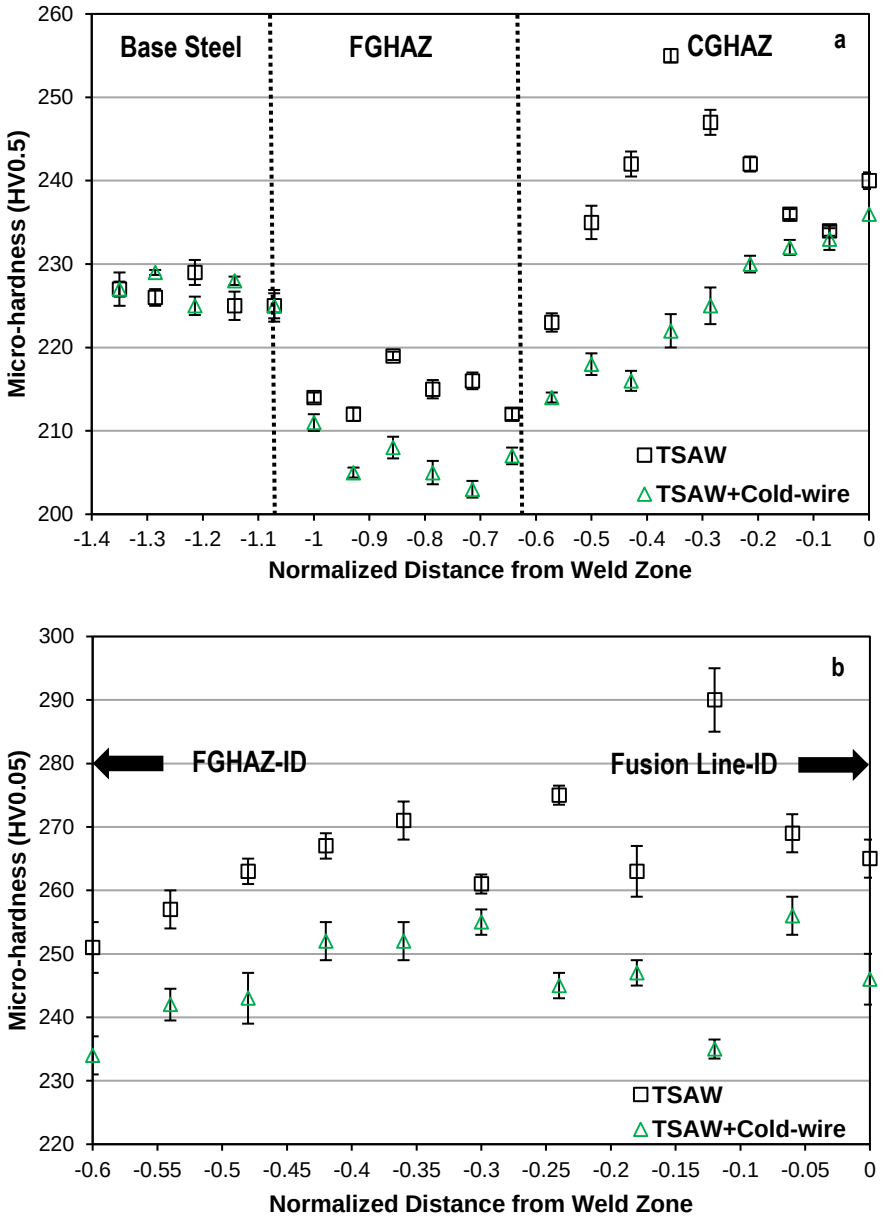

Figure 2. Micro-hardness variation along the (a) HAZ of the OD weld and (b) ICRCGHAZ region.

The reduction in the micro-hardness value along the HAZ can be attributed to the microstructural alterations taking place during welding as a result of the reduction in the heat introduced to the weldment by the cold wire. In spite of the same nominal welding heat input for both OD welding processes, the introduction of a cold wire in the TSAW process (CW-OD weld) leads to a reduction in the heat introduced to the weldment due to consumption of the heat of the trail electrode. As such, the retention time in the austenite region

(1100-1400ºC) decreases with a corresponding increase in the cooling rate in the CGHAZ. In addition, cold wire addition during the OD weld results in a reduction in the retention time in the austenite/ferrite transformation temperature range (A_{C1} and A_{C3}) in the intercritical HAZ (ICHAZ). This then causes a reduction in the fraction of ferrite (formed primarily in the CGHAZ of the ID weld) that transforms to austenite by intercritical reheating during OD welding and consequent formation of a lower fraction of martensite with retained austenite (M-A constituents) in the ICRCGHAZ. The formation of the lower fraction of refined M-A constituents within the CGHAZ and the ICRCGHAZ results in a reduction in the micro-hardness. However, as stated earlier, due to the direct impact of M-A constituents on the fracture toughness of the ICRCGHAZ, a reduction in the M-A fraction could positively influence the fracture toughness of the ICRCGHAZ resulting from the TSAW+cold-wire process.

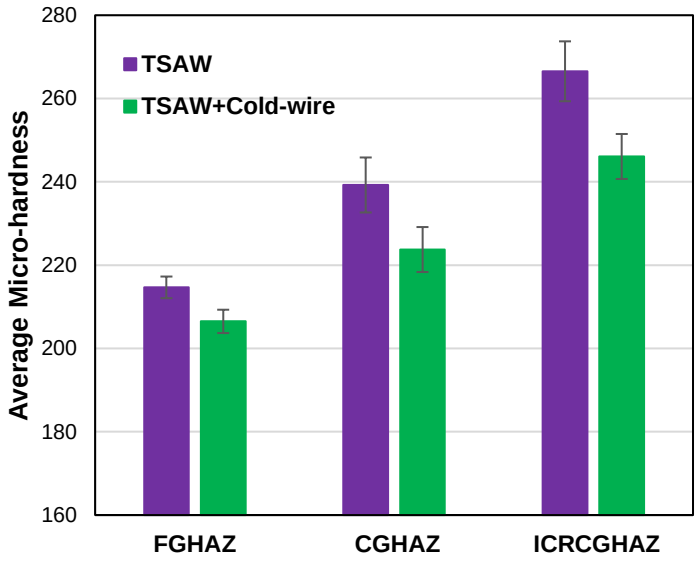

Figure 3. Average micro-hardness in the FGHAZ and CGHAZ and ICRCGHAZ of the OD weld for X70 steel.

3.2. Microstructure Characterization

TEOM and SEM micrographs of the CGHAZ of both CW-OD and TW-OD specimens at a location of 100 μm away from the fusion line of the OD weld are shown in Fig. 4a and 4c and 4b and 4d, respectively. Polygonal ferrite (PF) was identified as regions with no small phases within the grains (typically yellow in color), whereas granular GB was revealed as regions with a few small phases within the grains (typically brown in color). Bainitic ferrite (BF) and the M-A constituents are the dark brown and white regions, respectively, in the TEOM micrographs. The microstructure of the CGHAZ for both weld specimens consists of an inhomogeneous distribution of PF, GB, BF and M-A constituents. However, the presence of coarse M-A constituents is more pronounced in the CGHAZ of the TW-OD specimen compared with the CW-OD weld. The formation of M-A constituents in the CGHAZ is directly influenced by the PAG size

[24–26]. Grain size analysis (50-350 µm away from the fusion line of the OD weld) indicates a decrease in the PAG size in the CGHAZ from 60±5 µm for the TW-OD weld to 45±4 µm for the CW-OD weld. The reduction in the PAG size in the CGHAZ with cold wire addition is essentially attributed to lowering of the peak temperature and a decrease in the retention time within the austenitization temperature range (1100-1400°C) due to a decrease in the welding heat input and consequent increase in the cooling rate. The work done by Shome et al. [27] and Amer et al. [28] reported that the PAG size increased in the CGHAZ when the welding heat input was increased.

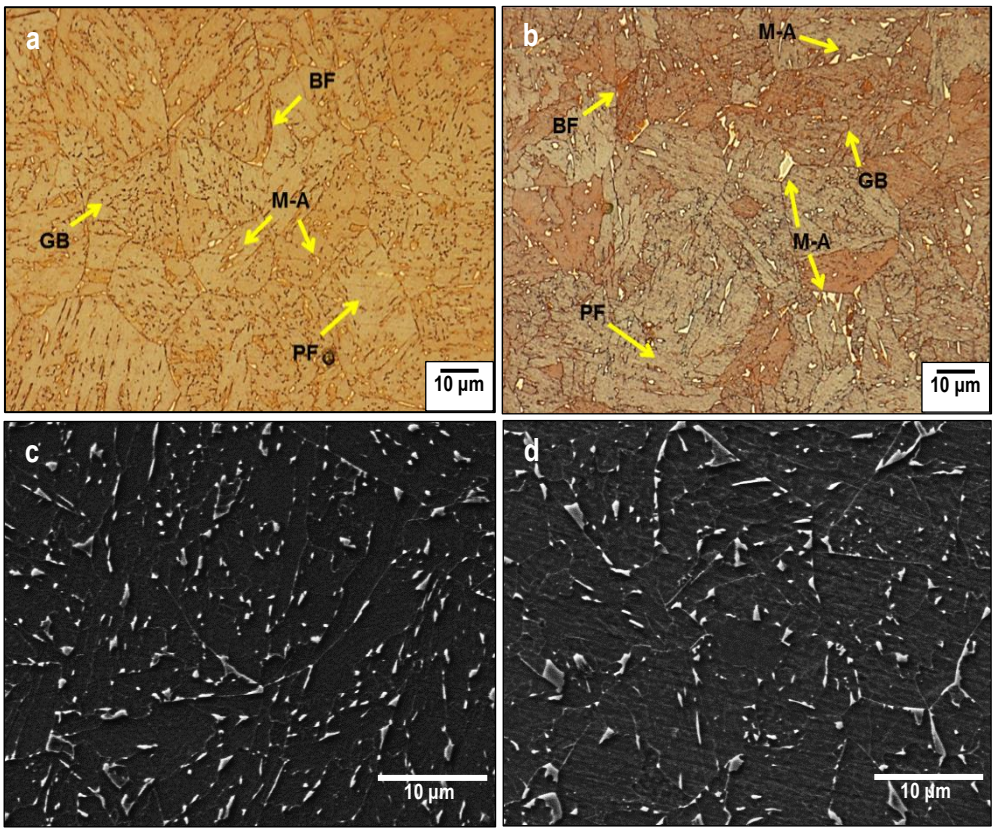

Figure 4. (a, b) TEOM and (c, d) SEM secondary electron (SE) micrographs of the CGHAZ of (a, c) the CW-OD weld and (b, d) the TW-OD weld. M-A constituents (white), PF (light brown), GB (light brown with tiny M-A islands with the grains) and BF (dark brown) were revealed by TEOM in (a) and (b). M-A regions in the SEM images ((c) and (d)) appear as white raised regions.

The average fraction of M-A constituents in the CGHAZ of the TW-OD and CW-OD welds (analyzed at three different locations of the CGHAZ of each weld) was measured as 4.2±0.2% and 3.1±0.1%, respectively. Quantitative analysis of the CGHAZ indicated that the fraction of M-A constituents longer than 2 µm for the TW-OD and CW-OD samples was 3.1±0.1% and 1.0±0.1%, respectively. According to the equation (Ms (ºC) = 542.3–30.0*G) proposed by Lee et al. [29], the martensite start (Ms) temperature

is linearly proportional to the ASTM PAG size number (G). The PAG size reduction in the CGHAZ by addition of the cold wire resulted in a decrease in the Ms temperature from ~407ºC (TW-OD weld) to ~370ºC (CW-OD weld). In addition, according to the Koistinen-Marburger [30] and Fisher et al. [31] models, the fraction of martensite is a function of the amount of undercooling below the Ms temperature. The fraction of martensite formed during the early stages of transformation of austenite is proportional to the cube of PAG size. As such, a higher fraction of larger M-A constituents is formed in the CGHAZ of the TW-OD weld relative to the CW-OD weld as a result of the higher Ms temperature and larger PAGs [31,32]. This phenomenon is confirmed by the work done by Hidalgo et al. [32], Heinze et al. [33] and Li et al. [26], where the fraction and size of martensite increased with increasing PAG size and, as such, the mechanical properties (strength, toughness and hardness) changed. Yu et al. [14] and Gharibshahiyan et al. [15] also reported that a microstructure consisting of coarse PAGs and coarse M-A constituents is the most detrimental one to the properties of the CGHAZ. The proportion of the local brittle zones increased with increased formation of M-A constituents in the CGHAZ of the TW-OD weld which resulted in higher micro-hardness values in the CGHAZ compared with the CW-OD weld. However, according to previous studies [24,25,34–36], the formation of coarser PAGs associated with a higher fraction of coarse M-A constituents resulted in deterioration in the fracture toughness of the CGHAZ of the TW-OD weld.

The microstructural features formed in the ICRCGHAZ of the CW-OD and TW-OD welds are shown in Fig. 5a and 5c, and 5b and 5d, respectively. EBSD micrographs of both the CGHAZ and ICRCGHAZ of the X70 steel welded by TSAW process (TW-OD weld) are shown in Fig. 6. For a given weld specimen, a higher density of M-A constituents (revealed as small black regions) is formed along the grain boundaries in the ICRCGHAZ compared with the CGHAZ. Furthermore, the fraction of slender shape M-A constituents formed in the ICRCGHAZ is higher than that in the CGHAZ. The grain boundary misorientation angle analysis showed that a higher fraction of ferrite/bainite grains with boundary angle greater than 15° was formed in the CGHAZ of the TSAW+cold-wire weld compared with that of the TSAW weld. The fraction of the various microstructural features formed in the CGHAZ and ICRCGHAZ is shown in Fig. 7a. As stated earlier, M-A constituents are believed to strongly impact the properties of both the CGHAZ and the ICRCGHAZ regions. A lower fraction of M-A constituents is formed in the ICRCGHAZ of the CW-OD weld (5.3±0.2%) relative to the TW-OD weld (7.5±0.3%). The additional cold wire in the TSAW of the OD weld results in a reduction in the actual welding heat input with a corresponding reduction in the retention time in the austenite/ferrite transformation temperature range (A_{C1}-A_{C3}) in the ICRCGHAZ, since much less ferrite is transformed to austenite and, consequently, a lower fraction of the M-A constituents is formed during cooling. According to the heat input analysis methodology described in [37], the heat input of the TSAW+cold-wire process was reduced by 10% relative to TSAW with a corresponding increase of 9% in the cooling rate.

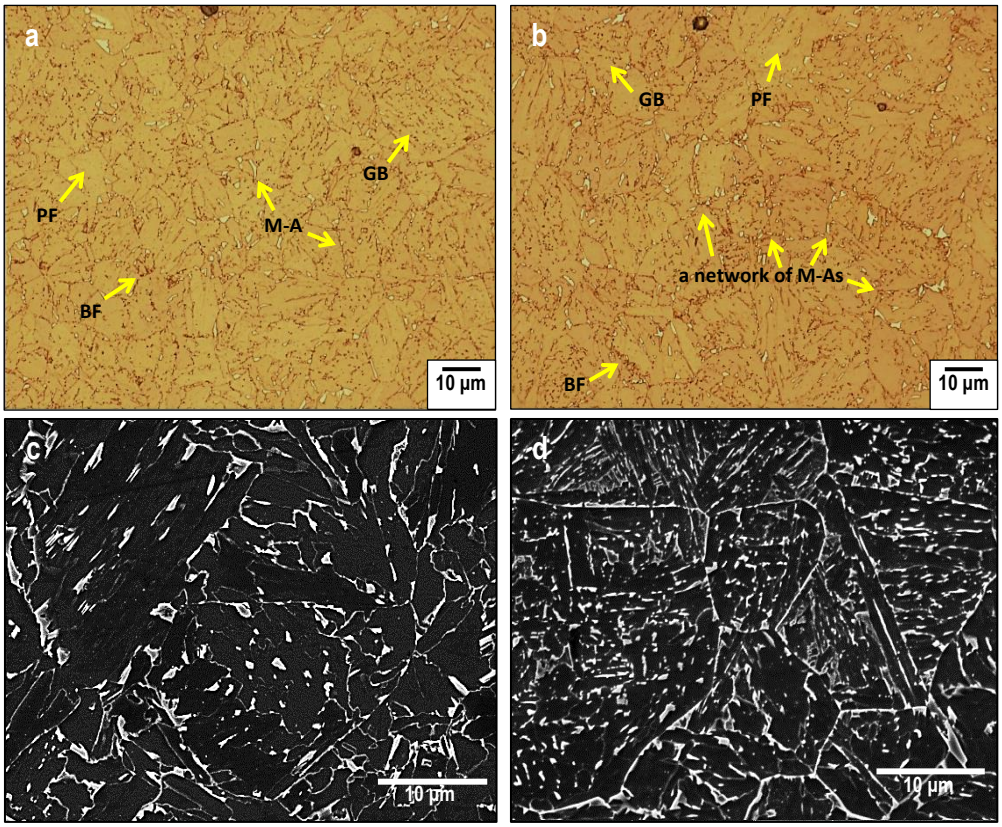

Figure 5. (a, b) TEOM and (c, d) SEM SE micrographs of the ICRCGHAZ of the (a, c) CW-OD and (b, d) TW-OD welds.

In addition to the M-A fraction, other characteristics of the M-A constituents, i.e., shape, size, distribution and aspect ratio (length/width), play a significant role on the mechanical properties of the CGHAZ and the ICRCGHAZ. As shown in Fig. 4, coarser M-A with slender shapes are formed in the CGHAZ of TW-OD weld due to the larger PAGs (as a result of the relatively higher heat input) compared with the M-A in the CW-OD weld. Analysis of the length and aspect ratio distribution of the M-A constituent (Fig. 8a-d) shows that more M-A constituents that are longer and have larger aspect ratios are formed in the CGHAZ of the CW-OD weld, which is due to the larger PAGs (as a result of the relatively higher heat input) compared with the TW-OD weld.

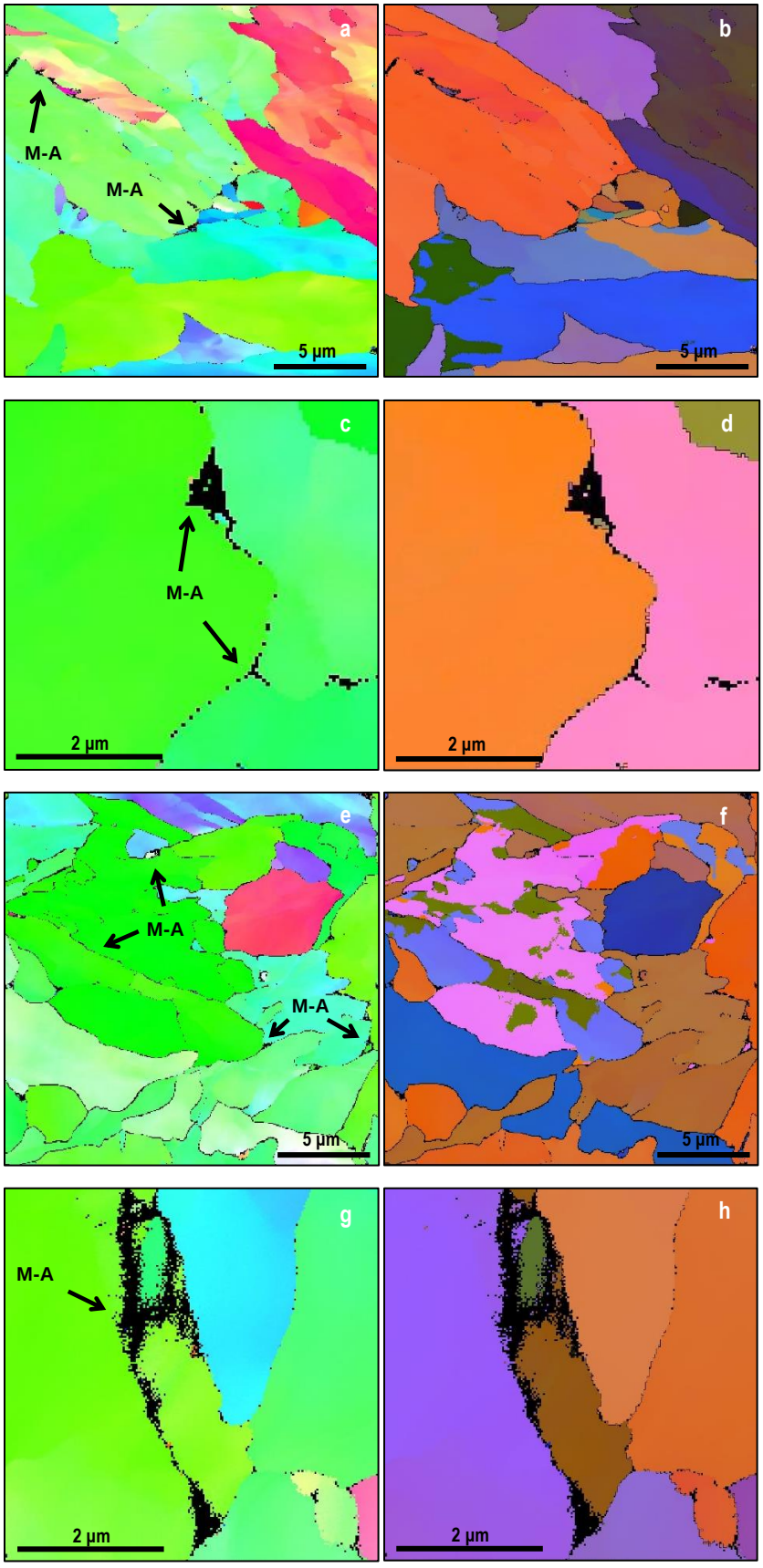
a
M-A
M-A
5 μm
b
5 μm
c
M-A
2 μm
d
2 μm
e
M-A
M-A
5 μm
f
5 μm
g
M-A
2 μm
h
2 μm

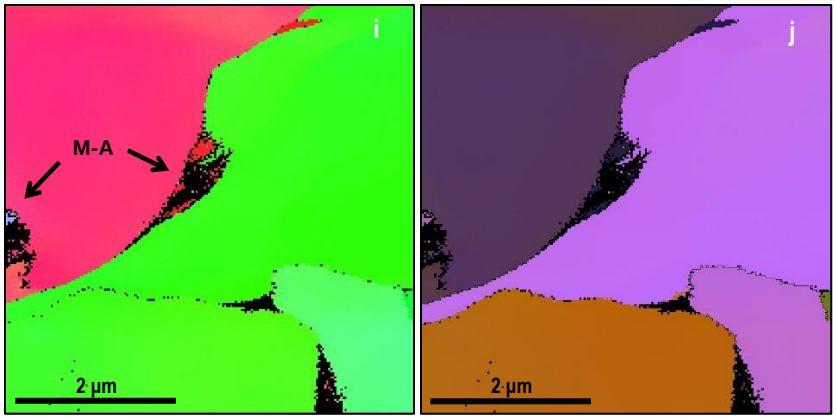

Figure 6. EBSD micrographs indicating M-A constituent distribution (black regions) in the (a-d) CGHAZ and (e-j) ICRCGHAZ of welded X70 microalloyed steels. Grain boundaries with the angle greater than 10º are highlighted in (b, d, f, h, j). The M-A constituents are comprised of a mixture of two different phases, i.e., austenite (FCC crystal structure) and martensite (essentially a BCC crystal structure with slight distortion in the c direction due to supersaturation by carbon), which result in the identification of small regions that do not correspond to the matrix phase.

With reference to the ICRCGHAZ, it is generally accepted that the formation of a necklace structure of large M-A constituents results in deterioration of the mechanical properties. However, the microstructural characteristics and consequent mechanical properties in the ICRCGHAZ of welded microalloyed steel are significantly influenced by the heat input of the second welding pass. As shown in Fig. 5, the fraction and size of M-A constituents are decreased in the ICRCGHAZ of the CW-OD weld. Moreover, a lower fraction of M-A constituents is formed along the PAG boundaries in the ICRCGHAZ of the CW-OD weld relative to the TW-OD weld. The length and aspect ratio distribution analysis of the M-A constituent in the ICRCGHAZ of the weld specimens, shown in Fig. 8e-h, showed that the number of M-A constituents with greater length and aspect ratio was higher in the ICRCGHAZ of the TW-OD weld compared with the CW-OD weld. The mean size and aspect ratio of M-A constituents in the CGHAZ and ICRCGHAZ of both the CW-OD and TW-OD welds are shown in Fig. 7b. The size and aspect ratio of the M-A constituents are larger in both regions for the TW-OD weld compared with the CW-OD weld. These affects are attributed to the lower actual heat input of the OD weld by cold wire addition (CW-OD weld) and the resultant faster cooling rate and shorter retention time in the austenitization temperature range (for the CGHAZ region) and the A_{C1}-A_{C3} temperature range (for the ICRCGHAZ region). The microstructure formed in the CGHAZ and ICRCGHAZ of the TW-OD weld with high fraction of slender M-A constituents formed along boundaries is more susceptible to the formation of micro-cracks and, consequently, deterioration in the mechanical properties, particularly toughness [3,38,39].

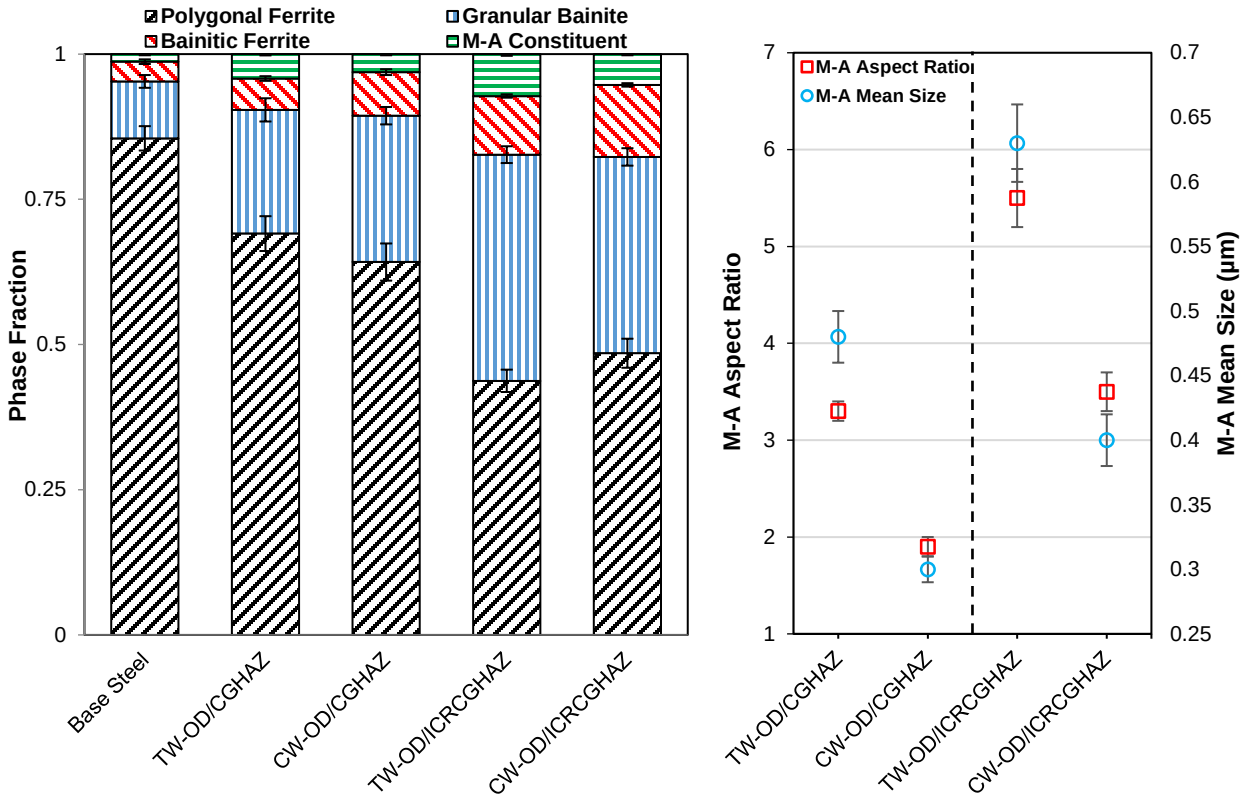

Figure 7. (a) Fraction of the various microstructural features and (b) mean size (equivalent spherical diameter) and aspect ratio of the M-A constituents formed in the CGHAZ and ICRCGHAZ of CW-OD and TW-OD welds.

The work done by Luo et al. [40], Wang et al. [41] and Bonnevie et al. [42] showed that the thermal cycle of the second welding pass results in the alterations in the characteristics of M-A constituents in the ICRCGHAZ. It was reported that a higher fraction of M-A constituents with slender shapes were formed in the ICRCGHAZ at higher welding heat inputs (i.e., slower cooling rates) which were detrimental to the fracture properties. The work done by Li et al. [43] showed that slender M-A constituents containing segregated alloying elements, such as carbon and manganese, were detrimental to the fracture toughness of the ICRCGHAZ.

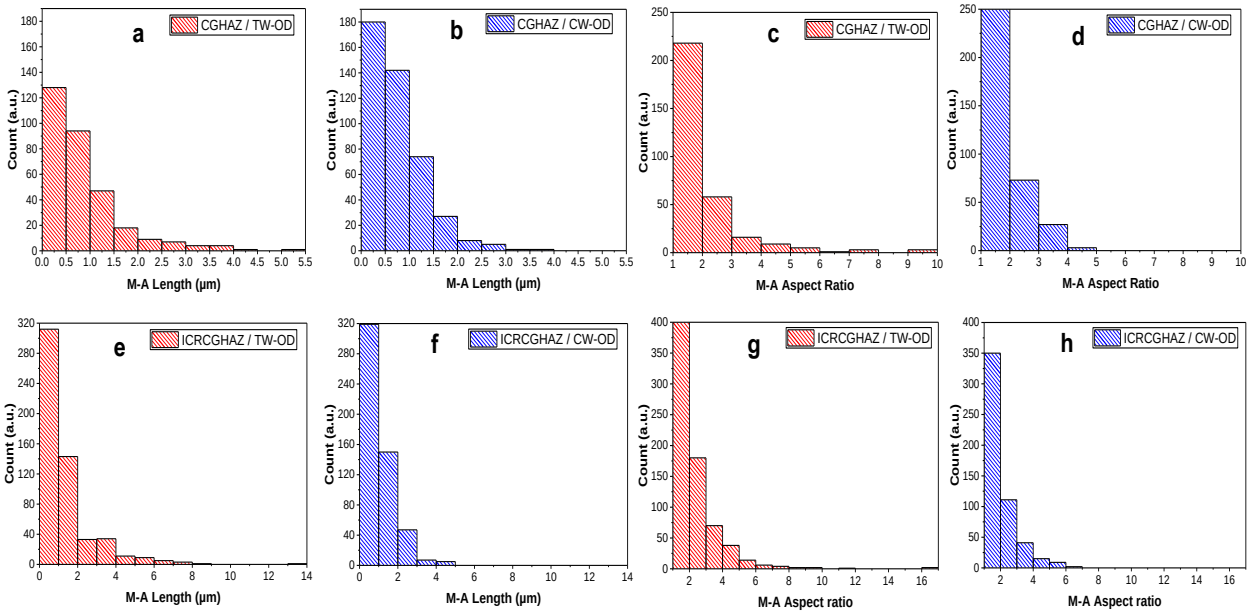

Figure 8. Distribution analysis of M-A constituent length (a, b, e, f) and aspect ratio (c, d, g, h) in the CGHAZ (a-d) and ICRCGHAZ (e-h) of the CW-OD and TW-OD welds.

Fig. 9a shows a TEM bright field (BF) micrograph of a blocky M-A constituent that has formed in the ICRCGHAZ of the CW-OD weld specimen. Selected area electron diffraction (SAED) patterns were extracted from the M-A constituent and the ferritic matrix and are shown in Fig. 9b and 9c, respectively. The pattern shown in Fig. 9b is from the M-A region indicated in Fig. 9a and can be indexed to austenite with an orientation corresponding to the [001] zone axis. The satellite spots in Fig. 9b are due to multiple diffraction, which will be discussed in the next paragraph. The pattern in Fig. 9c is from an adjacent ferrite grain at the same specimen orientation as Fig. 9b, which is not a zone axis for ferrite. Bright field and dark field images of a long slender shaped M-A constituent are shown in Fig. 10a and 10b, respectively. Corresponding electron diffraction patterns from the M-A regions are shown in Fig. 10c and 10d. The patterns can be indexed to the [0$\underline{1}$1] and [001] zone axes of austenite and contain satellite spots.

Martensite formed from austenite during cooling in the CGHAZ and ICRCGHAZ of welded microalloyed steels is always coupled with austenite retained through the transformation of austenite to martensite, which results in the formation of a dual phase microstructure, known as M-A constituent. The retained austenite, however, has a lower dislocation density compared with martensite and bainite/ferrite [44]. The work done by Lambert et al. [35] reported that retained austenite could form along the periphery of the MA islands with martensite forming at the center due to a chemical and/or mechanical stabilization mechanism. However, Yu et al. [14] and Hrivnak et al. [44] reported the existence of small retained austenite regions within the M-A regions and martensite regions dispersed throughout and along the edges of the M-A constituents, due to a high percentage of carbon and higher martensite start temperature [45,46]. As such,

the patterns from the M-A constituent (Fig. 9b, 10c and 10d) are due to diffraction from both austenite (FCC) and martensite. The satellite spots in the diffraction patterns are due to rediffraction of the diffracted beams travelling through the crystal. Fig. 11 depicts a schematic representation of the multi-diffraction phenomenon for the specific pattern in Fig. 9b. Initially, the incident beam travelling through M-A constituent is diffracted by several planes within austenite (FCC), generating the zone axis pattern shown in Fig. 11a. The incident beam is also diffracted by the martensite (essentially a BCC crystal structure) underneath austenite. Here, martensite is not oriented along the zone axis, so only a few spots are generated (Fig. 11b). Each diffracted beam from austenite can act as an incident beam for the martensite below. Therefore, each diffracted beam from austenite generates its own martensite diffraction pattern (satellite spots). This process is shown in Fig. 11c for one diffracted spot; however, rediffraction of each diffracted beam results in the generation of the multiple satellite spots in the SAED pattern (Fig. 11d).

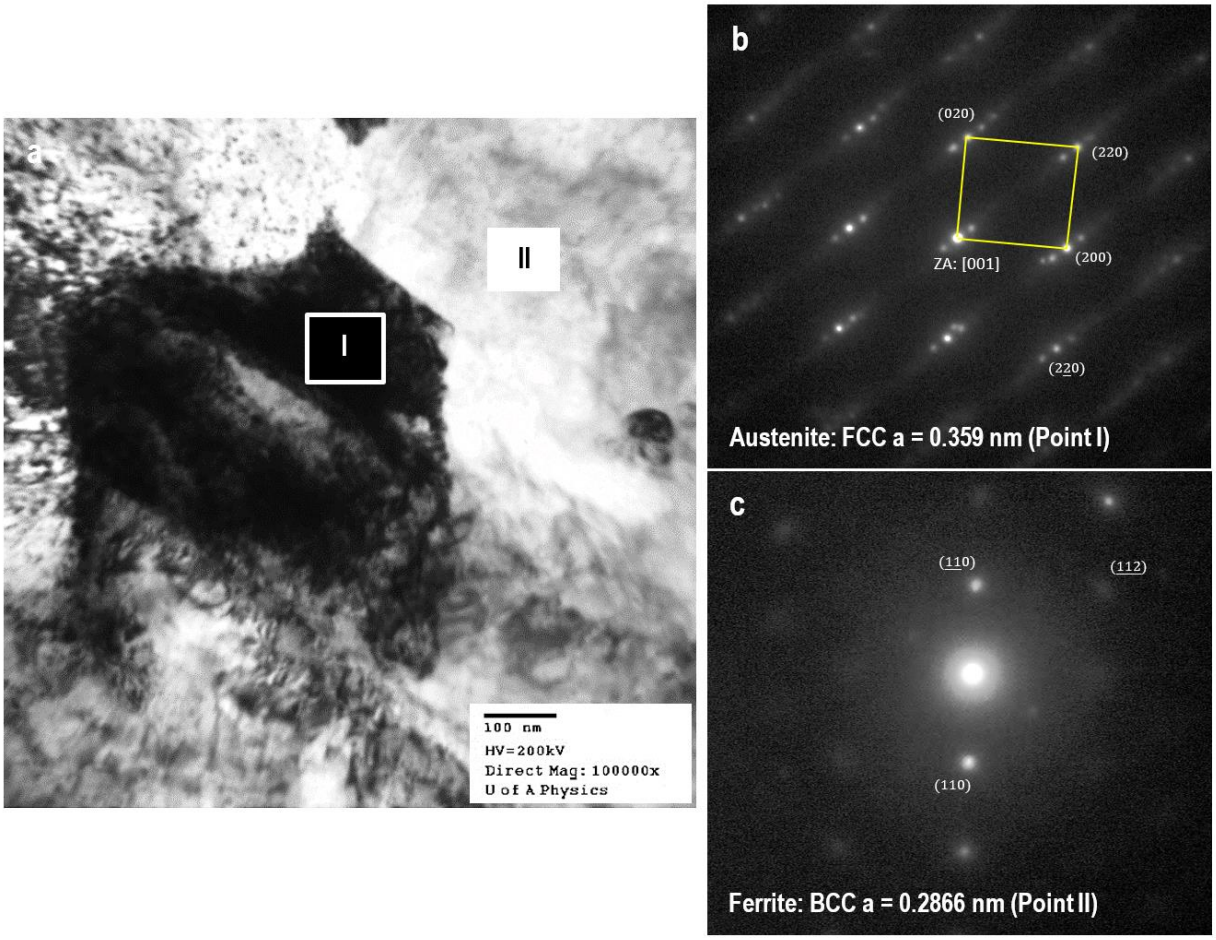

Figure 9. (a) TEM BF image of a blocky M-A constituent (I) formed in the ferritic matrix of the ICRCGHAZ of the CW-OD weld. SAED patterns from the (b) M-A island (I) and (c) ferrite grain (II) of the matrix.

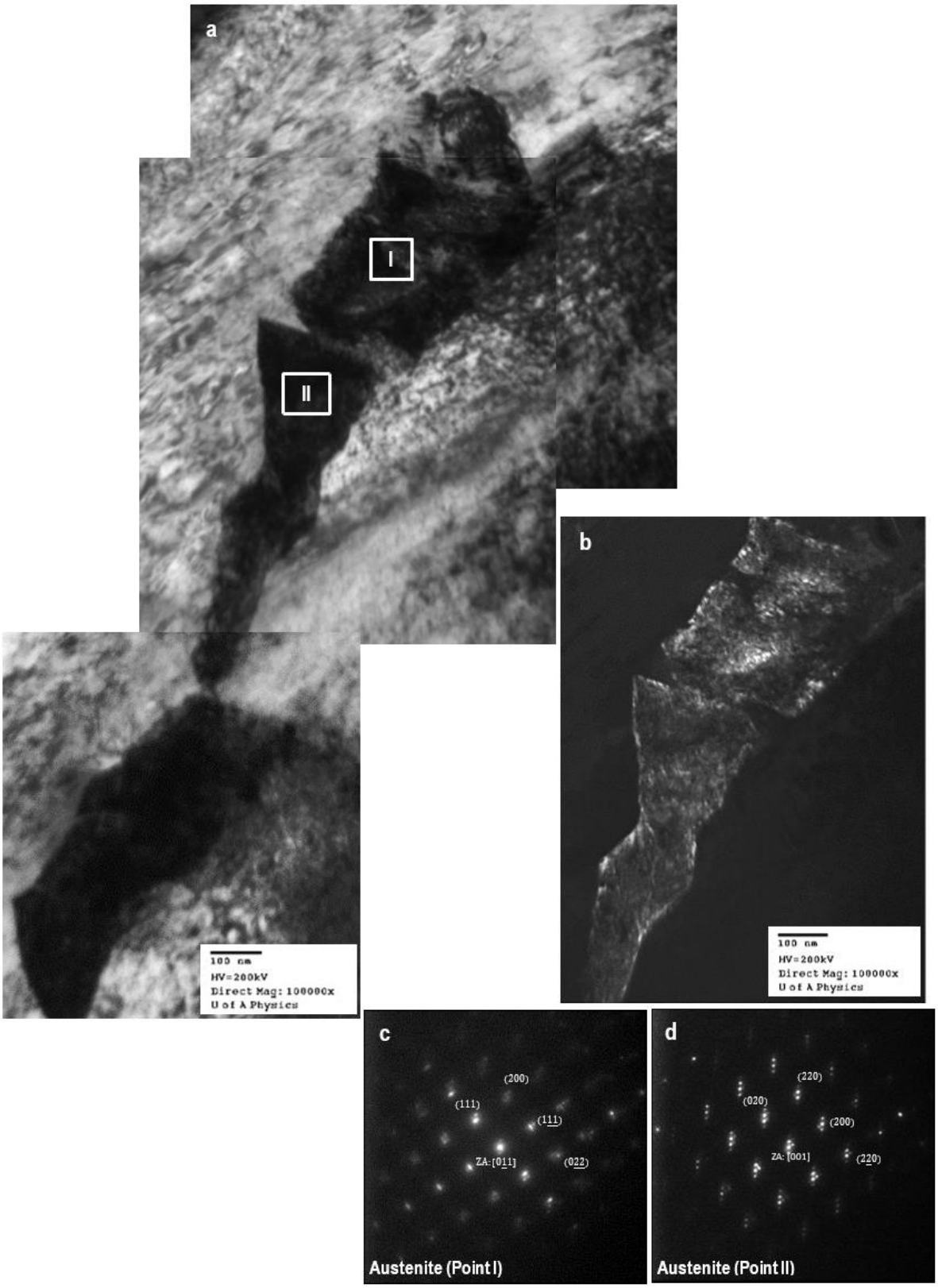

Figure 10. (a) BF TEM image and (b) DF TEM image of a continuous network of connected slender M-A constituents. (c, d) SAED patterns from the M-A region.

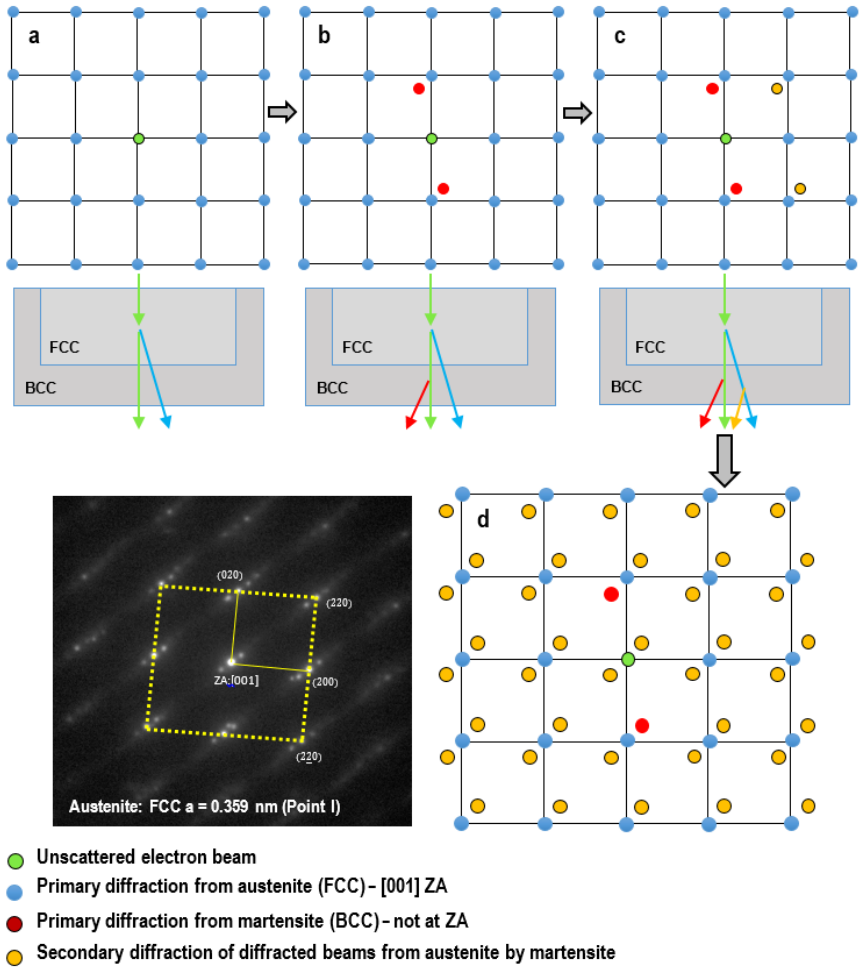

Figure 11. Schematic of the sequence of formation of SAED pattern from a typical M-A constituent; the pattern is Fig. 9b is used as a specific example. (a) Primary diffraction from austenite, (b) primary diffraction from martensite below austenite, (c) secondary diffraction and (d) final diffraction pattern generated from the M-A region.

4. Conclusions

The microstructure and micro-hardness in the coarse grained heat affected zone (CGHAZ) and the intercritical reheated CGHAZ (ICRCGHAZ) of an X70 microalloyed steel welded by a recently developed welding process, tandem submerged arc welding (TSAW) with additional cold wire (TSAW+cold-wire), and the conventional TSAW process were characterized. The formation of a lower fraction of fine M-A constituents associated with the smaller PAGs resulted in lower micro-hardness values along the CGHAZ of the steel welded by TSAW+cold-wire (CW-OD weld) relative to that welded by TSAW (TW-OD weld). In addition, the fraction of M-A constituents in the ICRCGHAZ of the CW-OD weld decreased. A higher fraction of slender shape M-A constituents in the ICRCGHAZ of the TSAW weld resulted in an increase in the micro-hardness. The changes in the microstructure characteristics and micro-hardness in the CGHAZ are essentially attributed to the reduction in welding heat input and an increase in the cooling rate with a

corresponding reduction in the retention time in the austenitic region (1100-1400ºC) by cold wire addition. Likewise, the reduction in heat input by the additional cold wire resulted in a reduction in the retention time in the ferrite/austenite region (A_{C1}-A_{C3}) and faster cooling rate in the ICRCGHAZ leading to the formation of a lower fraction of blocky M-A constituents and lower micro-hardness values in the ICRCGHAZ of the CW-OD weld sample.

Acknowledgments

The authors acknowledge the financial support from the Natural Sciences and Engineering Research Council (NSERC) of Canada, Evraz Inc. NA, TransCanada PipeLines Ltd., Enbridge Pipelines Inc., UT quality Inc. and Alliance Pipeline Ltd.

Data Availability

The raw/processed data required to reproduce these findings cannot be shared at this time due to legal or ethical reasons.

References

[1] V.G. Haugen, B.R.S. Rogne, O.M. Akselsen, C. Thaulow, E. Ostby, Local mechanical properties of intercritically reheated coarse grained heat affected zone in low alloy steel, Mater. Des. 59 (2014) 135–140. doi:DOI 10.1016/j.matdes.2014.02.010.

[2] Z. Zhu, L. Kuzmikova, H. Li, F. Barbaro, The effect of chemical composition on microstructure and properties of intercritically reheated coarse-grained heat-affected zone in X70 steels, Metall. Mater. Trans. B Process Metall. Mater. Process. Sci. 45 (2014) 229–235. doi:10.1007/s11663-013-0008-5.

[3] X.J. Di, X. An, F.G. Cheng, D.P. Wang, X.J. Guo, Z.K. Xue, Effect of martensite–austenite constituent on toughness of simulated inter-critically reheated coarse-grained heat-affected zone in X70 pipeline steel, Sci. Technol. Weld. Join. 21 (2016) 366–373. doi:10.1080/13621718.2015.1118814.

[4] Z. Zhu, J. Han, H. Li, Influence of Heat Input on Microstructure and Toughness Properties in Simulated CGHAZ of X80 Steel Manufactured Using High-Temperature Processing, Metall. Mater. Trans. A. 46 (2015) 5467–5475. doi:10.1007/s11661-015-3122-y.

[5] L. Lan, C. Qiu, D. Zhao, X. Gao, L. Du, Microstructural characteristics and toughness of the simulated coarse grained heat affected zone of high strength low carbon bainitic steel, Mater. Sci. Eng. A. 529 (2011) 192–200. doi:http://dx.doi.org/10.1016/j.msea.2011.09.017.

[6] S. Moeinifar, A.H. Kokabi, H.R.M. Hosseini, Effect of tandem submerged arc welding process

and parameters of Gleeble simulator thermal cycles on properties of the intercritically reheated heat affected zone, Mater. Des. 32 (2011) 869–876. doi:10.1016/j.matdes.2010.07.005.

[7] J. Hu, L.X. Du, J.J. Wang, H. Xie, C.R. Gao, R.D.K. Misra, High toughness in the intercritically reheated coarse-grained (ICRCG) heat-affected zone (HAZ) of low carbon microalloyed steel, Mater. Sci. Eng. A. 590 (2014) 323–328. doi:10.1016/j.msea.2013.10.062.

[8] S.Y. Han, S.Y. Shin, S. Lee, N.J. Kim, J.-H. Bae, K. Kim, Effects of Cooling Conditions on Tensile and Charpy Impact Properties of API X80 Linepipe Steels, Metall. Mater. Trans. A. 41A (2010) 329–340. doi:10.1007/s11661-009-0135-4.

[9] C.L. Davis, J.E. King, Effect of cooling rate on intercritically reheated microstructure and toughness in high strength low alloy steel, Mater. Sci. Technol. 9 (1993) 8–15.

[10] K.S. Kweon, J.H. Kim, J.H. Hong, C.H. Lee, Microstructure and toughness of intercritically reheated heat affected zone in reactor pressure vessel steel weld, Sci. Technol. Weld. Join. 5 (2000) 161–167. doi:10.1179/136217100101538155.

[11] S. Moeinifar, A.H. Kokabi, H.R. Madaah Hosseini, Influence of peak temperature during simulation and real thermal cycles on microstructure and fracture properties of the reheated zones, Mater. Des. 31 (2010) 2948–2955. doi:10.1016/j.matdes.2009.12.023.

[12] C.L. Davis, J.E. King, Cleavage Initiation in the Intercritically Reheated Coarse-Grained Heat-Affected Zone : Part I. Fractographic Evidence, Metall. Mater. Trans. A. 25 (1994) 563–573. doi:10.1007/BF02651598.

[13] W.W. XU, Q.F. WANG, T. PAN, H. SU, C.F. YANG, Effect of Welding Heat Input on Simulated HAZ Microstructure and Toughness of a V-N Microalloyed Steel, J. Iron Steel Res. Int. 14 (2007) 234–239. doi:https://doi.org/10.1016/S1006-706X(08)60085-0.

[14] L. Yu, H.H. Wang, T.P. Hou, X.L. Wang, X.L. Wan, K.M. Wu, Characteristic of martensite-austenite constituents in coarse grained heat affected zone of HSLA steel with varying Al contents, Sci. Technol. Weld. Join. 19 (2014) 708–714. doi:10.1179/1362171814Y.0000000246.

[15] E. Gharibshahiyan, A. Honarbakhsh, N. Parvin, M. Rahimian, The effect of microstructure on hardness and toughness of low carbon welded steel using inert gas welding, Mater. Des. 32 (2011) 2042–2048. doi:10.1016/j.matdes.2010.11.056.

[16] H.S. Yang, H.K.D.H. Bhadeshia, Austenite grain size and the martensite-start temperature, Scr. Mater. 60 (2009) 493–495. doi:10.1016/j.scriptamat.2008.11.043.

[17] A. Garcia-Junceda, C. Capdevila, F.G. Caballero, C. Garcia, D. Andre, Dependence of martensite start temperature on fine austenite grain size, Scr. Mater. 58 (2008) 134–137. doi:10.1016/j.scriptamat.2007.09.017.

[18] M. Mohammadijoo, S. Kenny, L. Collins, H. Henein, D.G. Ivey, Influence of cold-wire tandem

submerged arc welding parameters on weld geometry and microhardness of microalloyed pipeline steels, Int. J. Adv. Manuf. Technol. 88 (2017) 2249–2263. doi:10.1007/s00170-016-8910-z.

[19] N. Shikanai, S. Mitao, S. Endo, Recent Development in Microstructural Control Technologies through the Thermo-Mechanical Control Process (TMCP) with JFE Steel's High-Performance: JFE Technical Report No. 18 Plates, JFE Steel, Tokyo, 2007.

[20] B. De Meester, The weldability modern structural TMCP steels, ISIJ Int. 37 (1997) 537–551.

[21] ASTM, E3-11: Standard guide for preparation of metallographic specimens, ASTM International, PA, 2011. doi:10.1520/E0003-11.2.

[22] ASTM, E384-11: Standard test method for knoop and vickers hardness of materials, ASTM International, PA, 2012. doi:10.1520/E0384-11E01.2.

[23] F.S. LePera, Improved etching technique for the determination of percent martensite in high-strength dual-phase steels, Metallography. 12 (1979) 263–268. doi:10.1016/0026-0800(79)90041-7.

[24] X. Li, Y. Fan, X. Ma, S.V. Subramanian, C. Shang, Influence of martensite-austenite constituents formed at different intercritical temperatures on toughness, Mater. Des. 67 (2015) 457–463. doi:10.1016/j.matdes.2014.10.028.

[25] R. Cao, J. Li, D.S. Liu, J.Y. Ma, J.H. Chen, Micromechanism of Decrease of Impact Toughness in Coarse-Grain Heat-Affected Zone of HSLA Steel with Increasing Welding Heat Input, Metall. Mater. Trans. A. 46A (2015) 2999–3014. doi:10.1007/s11661-015-2916-2.

[26] X. Li, X. Ma, S.V. Subramanian, C. Shang, R.D.K. Misra, Influence of prior austenite grain size on martensite-austenite constituent and toughness in the heat affected zone of 700MPa high strength linepipe steel, Mater. Sci. Eng. A. 616 (2014) 141–147. doi:10.1016/j.msea.2014.07.100.

[27] M. Shome, Effect of heat-input on austenite grain size in the heat-affected zone of HSLA-100 steel, Mater. Sci. Eng. A. 445–446 (2007) 454–460. doi:10.1016/j.msea.2006.09.085.

[28] A.E. Amer, M.Y. Koo, K.H. Lee, S.H. Kim, S.H. Hong, Effect of welding heat input on microstructure and mechanical properties of simulated HAZ in Cu containing microalloyed steel, J. Mater. Sci. 45 (2010) 1248–1254. doi:10.1007/s10853-009-4074-7.

[29] S.-J. Lee, Y.-K. Lee, Effect of austenite grain size on martensitic transformation of a low alloy steel, Mater. Sci. Forum. 475–479 (2005) 3169–3172.

[30] D.P. Koistinen, R.E. Marburger, A general equation prescribing the extent of the austenite-martensite transformation in pure iron-carbon alloys and plain carbon steels, Acta Metall. 7 (1959) 59–60. doi:10.1016/0001-6160(59)90170-1.

[31] J.C. Fisher, J.H. Hollomon, D. Turnbull, Kinetics of the austenite-martensite transformation, Trans. Am. Inst. Min. Metall. Eng. 185 (1949) 691–700.

[32] J. Hidalgo, M.J. Santofimia, Effect of prior austenite grain size refinement by thermal cycling on the microstructural features of as-quenched lath martensite, Metall. Mater. Trans. A. 47 (2016) 5288–5301. doi:10.1007/s11661-016-3525-4.

[33] C. Heinze, A. Pittner, M. Rethmeier, S.S. Babu, Dependency of martensite start temperature on prior austenite grain size and its influence on welding-induced residual stresses, Comput. Mater. Sci. 69 (2013) 251–260. doi:10.1016/j.commatsci.2012.11.058.

[34] Z. Ying-qiao, Effect of Heat Input on Microstructure and Toughness of Coarse Grain Heat Affected Zone in Nb Microalloyed HSLA Steels, J. Iron Steel Res. Int. 16 (2009) 73–80. doi:10.1016/S1006-706X(10)60014-3.

[35] a. Lambert, A. Lambert, J. Drillet, A.F. Gourgues, T. Sturel, A. Pineau, Microstructure of martensite-austenite constituents in heat affected zones of high strength low alloy steel welds in relation to toughness properties, Sci. Technol. Weld. Join. 5 (2000) 168–173. doi:10.1179/136217100101538164.

[36] B. Hutchinson, J. Komenda, G.S. Rohrer, H. Beladi, Heat affected zone microstructures and their influence on toughness in two microalloyed HSLA steels, Acta Mater. 97 (2015) 380–391. doi:doi:10.1016/j.actamat.2015.05.055.

[37] M. Mohammadijoo, L. Collins, H. Henein, D.G. Ivey, Evaluation of cold wire addition effect on heat input and productivity of tandem submerged arc welding for low-carbon microalloyed steels, Int. J. Adv. Manuf. Technol. in press (2017) 1–13. doi:10.1007/s00170-017-0150-3.

[38] G. Spanos, R.W. Fonda, R.A. Vandermeer, A. Matuszeski, Microstructural changes in HSLA-100 steel thermally cycled to simulate the heat-affected zone during welding, Metall. Mater. Trans. A. 26A (1995) 3277–3293.

[39] M. Mohammadijoo, S. Kenny, L. Collins, H. Henein, D.G. Ivey, Effect of Cold-wire Addition in the TSAW Process on Microstructure and Mechanical Properties of the HAZ of X70 Microalloyed Pipeline Steel, Am. Soc. Mech. Eng. 3 (2016) 1–9. doi:10.1115/IPC2016-64549.

[40] X. Luo, X. Chen, T. Wang, S. Pan, Z. Wang, Effect of morphologies of martensite–austenite constituents on impact toughness in intercritically reheated coarse-grained heat-affected zone of HSLA steel, Mater. Sci. Eng. A. 710 (2018) 192–199. doi:https://doi.org/10.1016/j.msea.2017.10.079.

[41] X.L. Wang, X.M. Wang, C.J. Shang, R.D.K. Misra, Characterization of the multi-pass weld metal and the impact of retained austenite obtained through intercritical heat treatment on low temperature toughness, Mater. Sci. Eng. A. 649 (2016) 282–292. doi:https://doi.org/10.1016/j.msea.2015.09.030.

[42] E. Bonnevie, G. Ferrière, A. Ikhlef, D. Kaplan, J.M. Orain, Morphological aspects of martensite–

austenite constituents in intercritical and coarse grain heat affected zones of structural steels, Mater. Sci. Eng. A. 385 (2004) 352–358. doi:http://dx.doi.org/10.1016/j.msea.2004.06.033.

[43] X. Li, C. Shang, X. Ma, B. Gault, S. V. Subramanian, J. Sun, R.D.K. Misra, Elemental distribution in the martensite–austenite constituent in intercritically reheated coarse-grained heat-affected zone of a high-strength pipeline steel, Scr. Mater. 139 (2017) 67–70. doi:https://doi.org/10.1016/j.scriptamat.2017.06.017.

[44] I. Hrivnak, F. Matsuda, K. Ikeuchi, Investigation of M- A Constituent in High Strength Steel Welds, Trans. JWRI. 21 (1992) 149–171.

[45] C. Wang, X. Wu, J. Liu, N. Xu, Transmission electron microscopy of martensite/austenite islands in pipeline steel X70, Mater. Sci. Eng. A. 438–440 (2006) 267–271. doi:https://doi.org/10.1016/j.msea.2006.02.118.

[46] P. Zhang, Y. Chen, W. Xiao, D. Ping, X. Zhao, Twin structure of the lath martensite in low carbon steel, Prog. Nat. Sci. Mater. Int. 26 (2016) 169–172. doi:https://doi.org/10.1016/j.pnsc.2016.03.004.